analytical chemistry

Article

Liposome-assisted enzymatic modulation of plasmonic photoelectrochemistry for immunoassay

Feng-Zao Chen, De-Man Han, and Hong-Yuan Chen

Anal. Chem., **Just Accepted Manuscript** • DOI: 10.1021/acs.analchem.0c01162 • Publication Date (Web): 18 May 2020

is published by the American Chemical Society. 1155 Sixteenth Street N.W., Washington, DC 20036

Liposome-assisted enzymatic modulation of plasmonic photoelectrochemistry for immunoassay

Feng-Zao Chen,[1] De-Man Han,[2,*] Hong-Yuan Chen[1,*]

[1]State Key Laboratory of Analytical Chemistry for Life Science, School of Chemistry and Chemical Engineering, Nanjing University, Nanjing 210023, China

[2]Engineering Research Center of Recycling & Comprehensive Utilization of Pharmaceutical and Chemical Waste of Zhejiang Province, Taizhou University, Jiaojiang 318000, China

*To whom correspondence should be addressed.

*E-mail: hdmtzc@126.com

*E-mail: hychen@nju.edu.cn

ABSTRACT: Recently emerged liposomal photoelectrochemical (PEC) bioanalysis has brought new opportunities for biosensor development. This work presents the novel concept of liposome-assisted enzymatic modulation of the plasmonic photoelectrochemistry for PEC bioanalysis, which was exemplified by an Au nanoclusters (NCs) sensitized nanoporous TiO_2 nanotubes (Au NC@TiO_2 NT) photoelectrode and an alkaline phosphatase (ALP)-loaded liposomal immunoassay of heart-type fatty acid-binding protein (h-FABP) in the 96-well plate. After the sandwich immunorecognition and subsequent lysis treatment, the enzymatically generated ascorbic acid (AA) by the released ALP was directed to reduce Au^{3+} into Au nanoparticles (NPs) using the Au NCs as seeds, leading to the in situ change of the photoelectrochemistry of the electrode and corresponding reduction of the photocurrent. The depressed signal could be correlated to target concentration with good analytical performance in terms of sensitivity and selectivity. This work features the liposome-assisted enzymatic modulation of the plasmonic photoelectrochemistry, which provides a new protocol for general PEC bioanalysis development.

KEYWORDS: Photoelectrochemistry; Bioanalysis; Liposome; Enzyme; Plasmonic Modulation

INTRODUCTION

Based on semiconductor photoelectrodes, photoelectrochemical (PEC) immunoassay has received considerable attention due to its good analytical performance.[1-9] The design of the signal amplification strategy is crucial to obtain low limits of quantification and detection for PEC immunoassay.[10-12] To achieve signal amplification, numerous efforts have been made to develop various sandwich immunoassay protocols with the use of different labels, which are mainly limited to nanomaterials and catalytic enzymes.[13-16] For example, Dai et al. used the silver iodide-chitosan nanoparticle (SICNP) as peroxidase mimetic to catalyze the biocatalytic precipitation (BCP) reaction for the PEC biosensing of human interleukin-6 (IL-6).[17] Tang et al. used glucose oxidase (GOx) to catalyze the *in-situ* production of the electron donor for the PEC immunoassay of the carcinoembryonic antigen (CEA).[18] The attractive potential that PEC immunoassay offers for future protein assay has created a need to establish new signal amplification mechanisms.

Liposomes, which are spherical vesicles with phospholipid bilayers and hollow cavities, provide unique advantages in shipping guest species, e.g. genes, drugs, and fluorescence dyes, for various applications.[19-29] Furthermore, liposomes form a crucial component of biomolecule analysis because of the potential of signal amplification by tracing the liposome-contained reporters, a process that is significantly different from detecting the label auxiliary reaction in traditional bioanalyses. Recently, the potential for the use of liposomes has stimulated an emerging interest in the arena of PEC immunoassay. Using the enediol-ligands sensitizing TiO_2 NPs photoelectrode, we

have previously presented the concept of liposomal PEC bioanalysis.[30] Based on the *in-situ* generation of the electron donor, Zhuang and co-workers developed a split-type liposomal PEC immunoassay for sensing the HIV-$_{P24}$ antigen.[31] Using horseradish peroxidase (HRP)-encapsulated nanoliposomes, Liu et al. achieved a PEC immunoassay of ochratoxins via the HRP-trigger enzymatic etching of CdS in the presence of H_2O_2.[32]

Furthermore, the plasmonic photoelectrochemistry between noble metal nanoparticles (NPs) and semiconductors represents a unique signaling route for PEC bioanalysis. Zhang and co-workers used surface-plasmon resonance (SPR) at the Au NP surface to generate hot electrons to inject into the adjacent ZnO for developing a self-powered PEC biosensor of glutathione (GSH), in which the introduction of the Au/ZnO interface is beneficial to improving PEC performance.[33] Combining TiO_2 nanosheet films and Au@Ag nanorods with localized surface-plasmon resonance (LSPR), Zhang and co-workers exploited a plasmon-enhanced PEC sensor for mercury (II) detection.[34] Dai and co-workers prepared WS_2/Au NPs nanocomposites to construct a LSPR-enhanced PEC biosensor for MCF-7 cell detection, in which the LSPR of Au NPs improved the photoelectric conversion efficiency of WS_2 nanosheets to achieve amplification of the PEC signal.[35]

Significantly, as an effective photosensitizer, noble metal nanoclusters (NCs) have received increasing attention for biochemistry applications.[36-37] Noble metal NCs , which are different from noble metal NPs, consist of a characteristically unique atom-packing factor, a strong quantum confinement effect and a discrete

molecule-like band structure. Liu et al. developed an Au NPs/Au NCs/TiO_2 ternary system, in which Au NPs act as an electron relay mediator and Au NCs act as the plasmonic sensitizer, respectively. The Au NCs has a distinct HOMO-LUMO gap, and the LUMO level is located above the Femi level of the Au NPs and the conduction band (CB) of TiO_2. These characteristics allow for the electrons to be photoexcited and subsequently directly transferred to the TiO_2 CB, or first transferred to the Femi level of the Au NPs and then to the TiO_2 CB under visible light illumination.[38] Based on the properties of energy band levels for the Au NCs and electron tunneling processes, Yue and co-workers designed an Au NCs/gold electrode for the PEC bioanalysis of H_2O_2 and glucose.[39]

Inspired by these researches, this study presents a novel concept of the liposome-assisted enzymatic modulation of the plasmonic photoelectrochemistry for immunoassay. As shown in Scheme 1a, the sandwich immunological recognition was allowed within the 96-well plate to confine the liposome labels, which was followed by a lysis process to release the encapsulated alkaline phosphatase (ALP). Subsequently, as shown in Scheme 1b, the free ALP was directed to catalyze the hydrolysis of ascorbic acid 2-phosphate (AAP) to generate the reductive products (AA), which can reduce Au^{3+} into Au NPs *in-situ* with the use of Au NCs as seeds on the Au NC@TiO_2 nanotube (NT) photoelectrodes. This growth process breaks the initial equilibrium state of the Au NC@TiO_2 NT heterojunction, leading to a new Au NPs-involved synergistic system. Acute myocardial infarction (AMI) is a major public health concern and the world's main cause of morbidity and mortality.[40] As a

novel biomarker of the AMI, h-FABP has gained more and more attention in the early stage of the AMI diagnosis. Compared with normal physiological level of h-FABP (2-6 ng/mL in the plasma), the concentration of h-FABP rises continuously after AMI onset during 1-8 h, and returns to the normal level within 24-36 h.[41,42] Exemplified by h-FABP as a model target (Antigen, Ag), this immunoassay protocol exhibited excellent properties in terms of sensitivity and selectivity. Our research features the liposome-assisted enzymatic modulation of the plasmonic photoelectrochemistry for PEC bioanalysis, which has not been reported. The results of our study can provide a new horizon for the design and implementation of innovative liposome-assisted plasmonic PEC bioanalysis.

Scheme 1. (a) Illustration of the Confinement of the ALP-Loaded Liposome Labels by the Sandwich Immunorecognition in the 96-Well Plate, and (b) ALP Catalytic Growth of Au NCs on the Au NC/TiO_2 NT Photoelectrode.

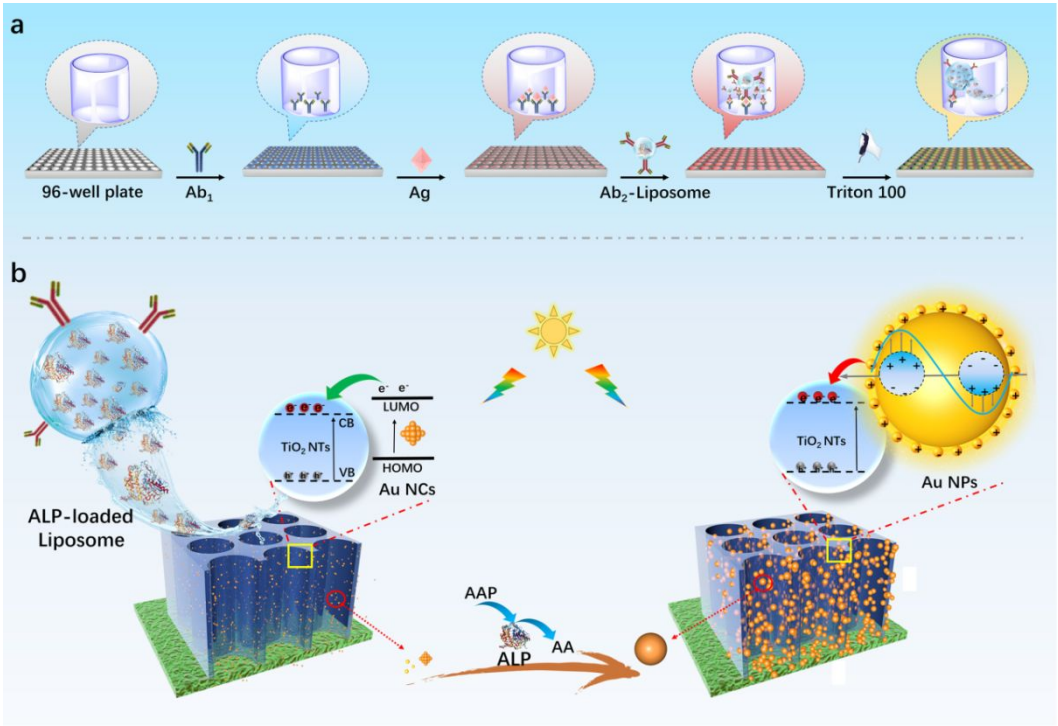

EXPERIMENTAL

Chemicals and Apparatus: All the regents used in this study were purchased from formal commercial suppliers not purified further. For more details on these products, please refer to the supporting information.

Fabrication of the Au NC@TiO_2 NT electrode. The Au NC@TiO_2 NT electrode was constructed according to previous literature with some subtle alteration.[38] The as-obtained TiO_2 NTs substrate electrode was pretreated with diluted hydrochloric acid. Subsequent to rinsing and drying with N_2, the TiO_2 NT electrode was dipped into an Au NCs solution for 8 h to obtain the Au NC@TiO_2 NT electrode. Details of the synthesis of TiO_2 NTs and Au NCs are contained in the supporting information.

Synthesis of the ALP-loaded Liposome. According to our previous work,[30] the process of bare liposome, ALP-loaded liposome (ALL) and Ab_2 conjugated ALP-loaded-liposome (Ab_2-ALL) were respectively prepared via the thin lipid film hydration and glutaraldehyde coupling method, which involved preparing a solution of cholesterol (7 mg), DPPE (5 mg), DPPG (15 mg), and DPPC (14.7 mg) in 12.8 mL of chloroform and 3.2 mL of methanol by vortex and ultrasound. The organic phase was then concentrated *in vacuo* to obtain the thin lipid film. 10 mL of ALP solution was added to hydrate the lipid film for overnight. The solution was subsequently prepared using ultrasound, filtered (via 0.45 μm and 0.2 μm polycarbonate filters), and modified with Ab_2. The resulting Ab_2-ALL was stored at 4 °C for further use.

Immunoassay development. 20 μL of Ab_1 (0.20 mg/mL) was added to the 96-well plates and allowed to incubate overnight at 4 °C. The well was then rinsed with a

washing buffer solution and the nonspecific binding sites were blocked via incubation with a BSA blocking buffer solution at 4 °C for 2 h. After being rinsed with the washing buffer solution, 30 μL of Ag at various concentrations was introduced into the 96-well plates and incubated at 4 °C for 1 h. A PBS buffer solution is then used to remove the uncombined Ag. Subsequently, 30 μL of Ab_2-ALL was added and the sample was incubated at 37 °C for 1 h. The well was then rinsed thrice using a PBS buffer solution. Finally, 30 μL of Triton X-100 (0.05 %) was added and incubated overnight at 4 °C. 20 μL of liposome lysate was then dropped onto the Au NC@TiO_2 NT electrode which contained Au^{3+} (0.02 %) and AAP (5 mM). After incubation at 37 °C for 1 h, the electrode was rinsed with a PBS buffer solution and measured using a photocurrent signal.

PEC measurements. PEC measurements were performed using a homemade PEC system. A CHI 660C electrochemical workstation was used as the electrochemical analyzer performed with a traditional three-electrode system: the Au NC@TiO_2 NT photoelectrode exposing a geometrical circular area (d = 4 mm) as the working electrode, with an Ag/AgCl and a Pt wire electrode as the reference electrode and the counter electrode, respectively. A 5 W LED lamp was used as the irradiation source to provide white light. All measurements were performed in a PBS (10 mM, pH = 7.4, containing 1 mM triethanolamine) buffer solution subsequent to settling for 3 minutes. The stability of the photoelectrode was performed by consecutive on-off light irradiation for several cycles during the measuring process. Specifically, the white light irradiation was provided to system every 10 s and lasted another 10 s.

RESULTS and DISCUSSION

Materials characterization. To construct an Au NC@TiO_2 NT photoelectrode, the precursor materials TiO_2 NTs and Au NCs were first prepared and then characterized. As shown in Figure 1a, the typical scanning electron microscope (SEM) top-view image presents the morphology of the prepared TiO_2 NTs. The TiO_2 NTs exhibit a regular NTs structure with uniform pores and clean surfaces. Figure 1b displays a typical transmission electron microscope (TEM) cross-section showing the structural features of the TiO_2 NTs, with a good conformity and ordered arrangement. The average outer pore diameter is 120 nm with a wall thickness of 20 nm. This unique three-dimensional nanostructure is beneficial for the light absorption and direct photo-induced electron transfer along the arrayed frameworks. Also, it is conducive to the subsequent accommodating of the Au NCs and can be flooded with electrolyte containing the involved molecules, ensuring short diffusion paths for these molecules and a high surface area for subsequent reaction. [43-45] Additionally, X-ray diffraction (XRD) patterns demonstrated that the crystal structure of the anatase-phase TiO_2 NTs was successfully fabricated (Figure 1c). Figure 1d shows the TEM image of the Au NCs, and the inset shows the corresponding size distribution histogram, with a peak at 1.8 nm. Figure 1e shows the UV-vis absorption spectra of the Au NCs solution, which exhibits a good absorption ability under visible light, with a characteristic absorption shoulder peak at approximately 405 nm. The Au NCs with a distinct LUMO-HOMO gap resemble semiconductors, and the energy gap (*Eg*) was calculated to be 2.88 eV (Figure S1). Figure 1f shows the excitation and fluorescence emission spectra of the

Au NCs. It reveals that the Au NCs are excited under UV-vis light in the range of 300 nm to 500 nm. The optimum excitation wavelength was observed at approximately 410 nm, and the corresponding fluorescence emission peak was at 575 nm. The fluorescence photograph can be clearly seen in the inset. Furthermore, the dependence of the zeta potential of the Au NCs samples against the various pH values was studied, and revealed the stability of the sample as shown in Figure S2.

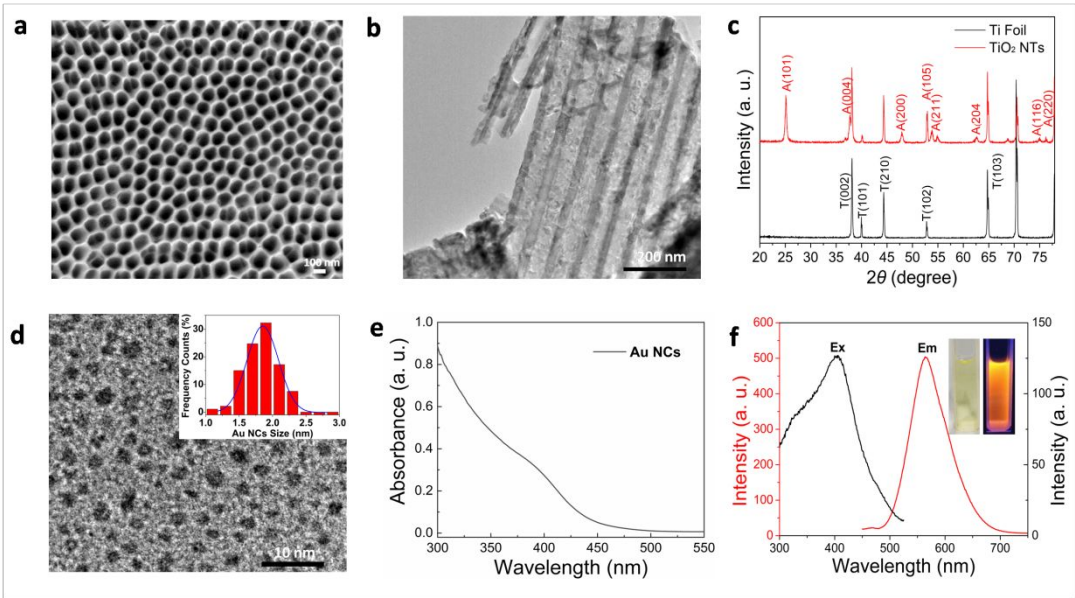

Figure 1. (a) SEM and (b) TEM image of bare TiO_2 NTs, respectively. (c) XRD patterns of Ti foil and TiO_2 NTs (A: Anatase, T: Ti foil). (d) TEM image of Au NCs. Inset: size distribution histogram of the Au NCs. (e) UV-vis absorption spectrum of Au NCs. (f) Excitation and fluorescence emission spectra of the Au NCs, Ex = 410 nm. Inset: photographs of Au NCs aqueous solution under "naked eye" and 365 nm UV light, respectively.

The obtained ALP-loaded liposome is approximately 60 nm and displays a quasi-spherical shape with unilamellar vesicles, as shown in Figure 2a. The dynamic light scattering (DLS) analysis revealed a narrow size distribution for the liposomes, with a hydrated diameter of around 105 nm (Figure 2b). The DLS of the bare and ALP-loaded liposomes were also investigated, and the results revealed that the

encapsulation of ALP does not affect the size of the liposomes (Figure S3). ALP-loaded liposomes were further investigated using an Alkaline Phosphatase Assay Kit to verify that ALP was successfully encapsulated in the liposomes and remained active. ALP can hydrolyze the chromogenic substrate, para-nitrophenyl phosphate, to *p*-nitrophenol, with a characteristic absorption peak at 410 nm.[46-47] Figure 2c records the UV-vis spectra of the bare liposome lysis solution (curve a), free ALP (curve b), and ALP-loaded liposome lysis solution (curve c) responding to the Alkaline Phosphatase Assay Kit. The bare liposome lysis solution showed no absorption, while the free ALP solution displayed a characteristic absorption peak at 410 nm. Subsequent to loading the ALP, it exhibited a similar characteristic absorption peak, indicating the successful fabrication of the ALP-loaded liposomes and the maintenance of favorable catalytic activity for the encapsulated ALP. Additionally, the zeta potential results, displayed in Figure 2d, suggest a high stability for the ALP-loaded liposomes. Additional characteristics of the liposomes are contained in the supporting information.

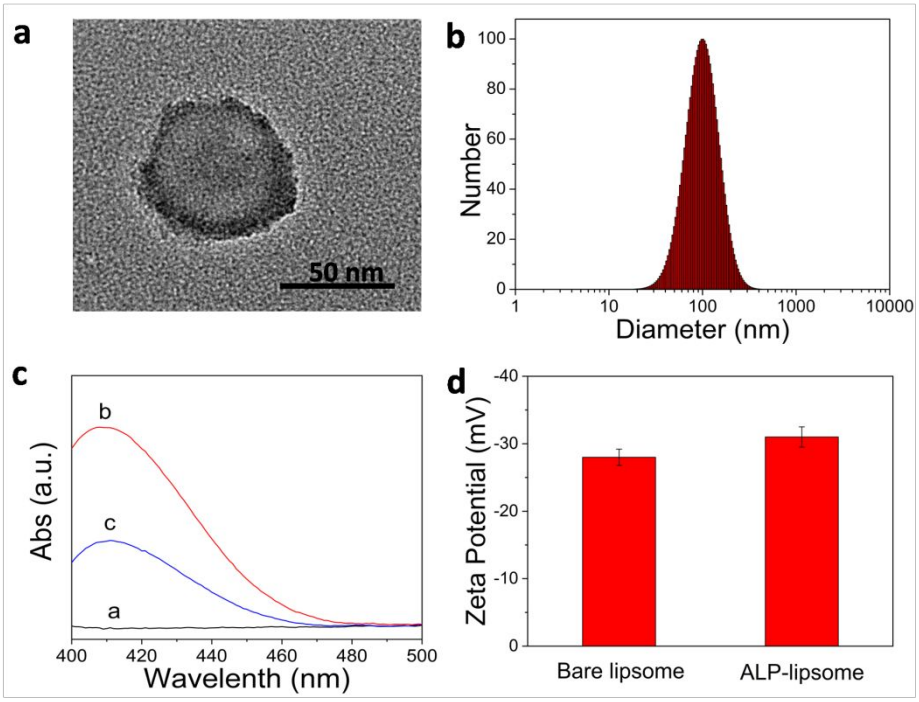

Figure 2. (a) TEM image of ALP-loaded liposome, and (b) corresponding DLS particle size distribution. (c) UV-vis absorption spectra for response of bare liposome lysis solution (curve a), free ALP (curve b), and ALP-loaded liposome lysis solution (curve c) to Alkaline Phosphatase Assay Kit, respectively. (d) Zeta potentials of the liposomes before and after loaded ALP.

The Au NC@TiO_2 NT photoelectrode was subsequently fabricated using porous TiO_2 NTs as a substrate to anchor the Au NCs. As shown in Figure 3a, the successful coupling of Au NCs on the TiO_2 NTs was confirmed via TEM images. It can be clearly observed that a number of high-contrast Au NCs were distributed on the TiO_2 NT electrode surface. Figure 3b further reveals the even distribution of the Au element on the TiO_2 NT photoelectrode. UV-vis diffuse reflectance spectra (DRS) were recorded to evaluate the optical properties of TiO_2 NTs prior and subsequent to coupling with Au NCs. As shown in Figure 3c, the Au NC@TiO_2 NTs exhibits distinct enhanced light harvesting in comparison with the blank TiO_2 NTs, which suggested that the existence of Au NCs on TiO_2 NTs can promote the light absorption of the photoelectrode in the visible light region. The absorption peak of bare TiO_2 NTs

at around 520 nm may be attributed to its specific nanoarray structure.[45] XPS spectra verifies the coexistence of Au 4f, Ti 2p, C 1s, and O 1s in the Au NC@TiO_2 NT electrode (Figure 3d). The high-resolution XPS analysis of O 1s, Ti 2p and Au 4f can be seen in the Figure 3e. The characteristic peaks located at 529.7 eV, 531.3 eV, and 533.1 eV can be attributed to Ti-O, Ti-OH, and carboxyl ($-COO^-$), respectively. The Ti $2p_{3/2}$ of Au NC@TiO_2 NTs shows a characteristic peak at 458.5 eV, which suggests that the Ti element is in the +4-oxidation state. Also, Ti displays a shift of *ca.* 0.4 eV for Ti $2p_{3/2}$ compared to bare TiO_2 NTs, which may arise from the intimate interfacial interaction between the Au NCs and TiO_2 NTs framework.[48] Characteristic peaks of Au are located at 84.1 eV, 87.8 eV, 336.0 eV, and 352.4 eV, and correspond to Au $4f_{7/2}$, Au $4f_{5/2}$, Au $4d_{5/2}$, and Au $4d_{3/2}$, respectively.[49] These results match well each other and suggest the successful fabrication of the Au NC@TiO_2 NT electrode.

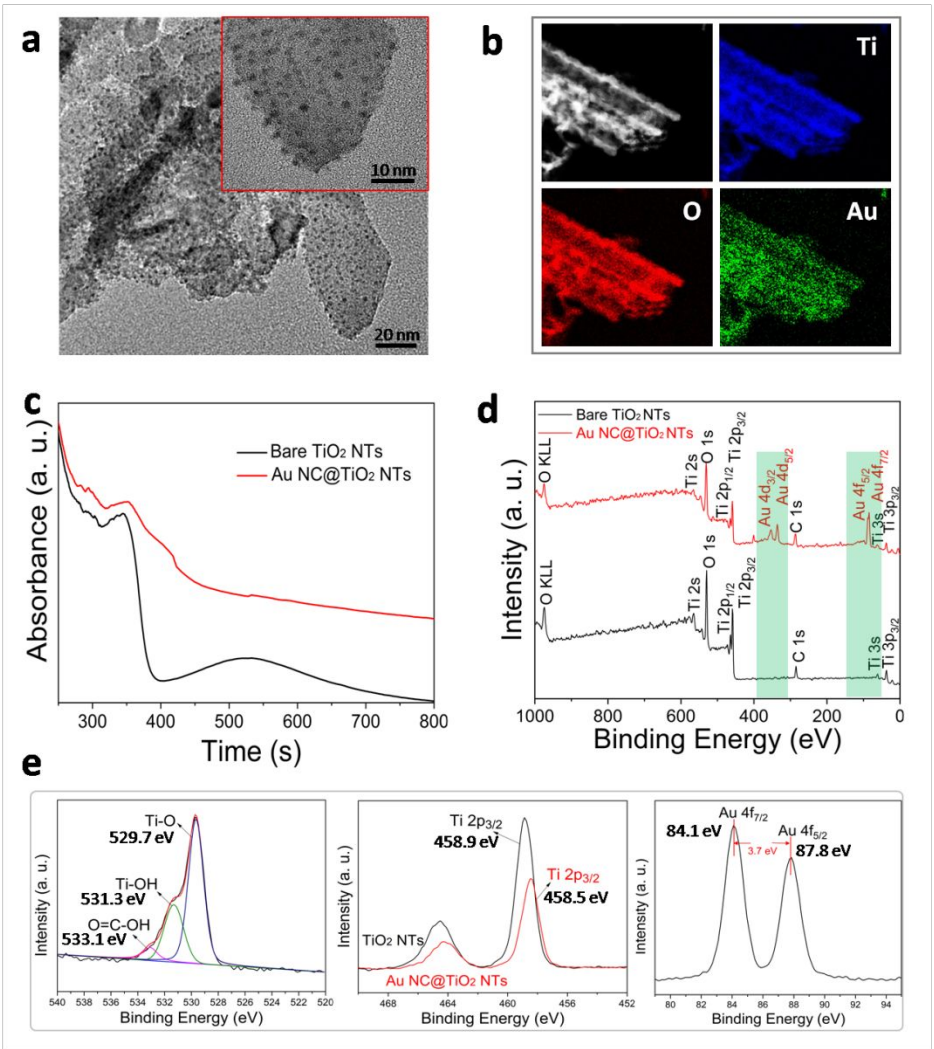

Figure 3. (a) TEM image of Au NC@TiO_2 NTs, and (b) corresponding EDS mapping. (c) UV-vis DRS of blank TiO_2 NTs (black curve) and Au NC@TiO_2 NTs (red curve). (d) Survey XPS spectra of the blank TiO_2 NTs and Au NC@TiO_2 NTs, and (e) corresponding high-resolution XPS spectra of O1s, Ti 2p, and Au 4f.

PEC Immunoassay Development and Feasibility Investigation. The PEC properties of the electrode were investigated by transient photocurrent responses spectra under intermittent visible light excitation. Figure 4a shows the chronoamperometric *i-t* responses of the blank TiO_2 NTs electrode (curve a), Au NC@TiO_2 NT electrode (curve b), and after incubation with the ALP (curve c) from liposomes corresponding to 10 ng mL^{-1} of h-FABP, respectively, under visible light irradiation. Distinctly, the blank TiO_2 NTs electrode showed an extremely weak photo

response due to its broad-band-gap, while obvious current signals appeared subsequent to coupling with Au NCs. However, after this electrode was incubated with the liposome lysis solution, the photocurrent signal dropped sharply. This may be attributed to the *in-situ* modulation of the plasmonic sensitization after Au NCs grew into Au NPs. The control experiments were performed to evaluate the influence of the ALP, AAP, and Au^{3+} species in this detection system. The results reveal that either single or any two species have only a negligible impact on the system, as illustrated in Figure S4. Additionally, the stability of the Au NC@TiO_2 NT electrode was studied and the result exhibited a reproducible response during 400 s (Figure 4b). UV-vis DRS was further applied to probe the changes in the absorbance spectra of the Au NC@TiO_2 NT electrode before (curve a) and after (curve b) reacting with the liposome lysis solution (Figure 4c). A characteristic absorption peak at 570 nm was observed, which is attributed to the SPR of the newly formed Au NPs. For better clarity, the morphological evolution of the Au NC@TiO_2 NT electrode was characterized by SEM and TEM. As shown in Figure 4d, after reacting with the lysis solution, the surface of the TiO_2 NTs became rough, followed by the appearance of numerous Au NPs with different shapes and sizes. These Au NPs spread throughout the nanotubes, as illustrated in Figure 4e. This observation suggests that the Au NCs deposited on the TiO_2 NTs surface not only enhance the photoelectrode's ability to harvest visible light, but also act as a crystalline seed for inducing the *in-situ* growth of Au NPs.

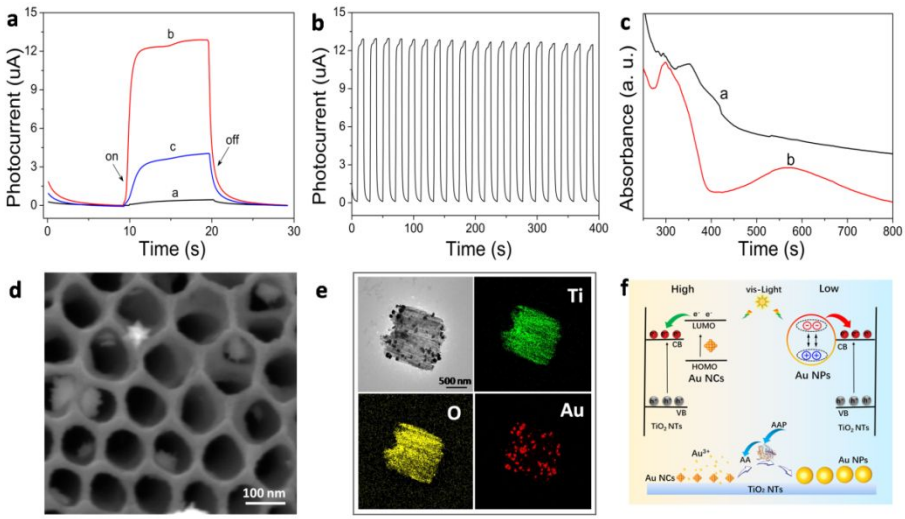

Figure 4. (a) Photocurrent response of TiO_2 NTs (curve a), Au NC@TiO_2 NTs before (curve b) and after (curve c) incubation with the ALP from liposome lysis solution. (b) Time-dependent current signal on Au NC@TiO_2 NT photoelectrode for 20 cycles on-off irradiation during 400 s. (c) UV-vis DRS of Au NC@TiO_2 NTs before (curve a) and after (curve b) incubation with the liposome lysis solution. (d) SEM image of Au NC@TiO_2 NTs after incubation with lysis solution, and (e) TEM image and EDS mapping. (f) Proposed mechanism for the photocurrent response. The PEC tests were performed in a PBS (10 mM, pH 7.4) buffer solution with 1 mM triethanolamine (TEA) as electron donor. 0 V versus Ag/AgCl applied-voltage and 5 W white-light LED were applied.

Based on our results, these PEC response behaviors can be attributed to the liposome-assisted enzymatic modulation of the plasmonic effect, as illustrated in Figure 4f. The CB of TiO_2 NTs is below the LUMO level of Au NCs, therefore the photoinduced electrons of the LUMO level can rapidly transfer to the CB of the TiO_2 NTs, thus resulting in a stable generation of anode current signal. The free ALP generated from the lysis solution was directed to catalyze the hydrolysis of ascorbic acid AAP. This generated the reductive products (AA), which reduces Au^{3+} into Au NPs *in-situ*, using Au NCs as the crystalline seeds on the Au NC@TiO_2 nanotubes (NTs) photoelectrode. It is noted that the location of the Femi level of the Au NPs above the CB of the TiO_2 NTs resulted the SPR-induced "hot electrons" could

transfer to the CB of the TiO_2 NTs. However, the triggering of the SPR effect of Au NPs need a specific excitation wavelength. In this work, we used white-light as the irradiation source rather than a specific monochromatic light. Thus, compared with the Au NCs, the contribution of Au NPs towards photocurrent intensity was much lower under white light irradiation in this system.

Performance of the Au NC@TiO_2 NT PEC biosensor. Since the degree of enzymatic modulation is closely associated with the amount of ALP-loaded liposome, a novel liposome-assisted PEC immunoassay can be achieved by recording the photo response current signal to monitor the immunoreaction. As shown in Figure 5a, an increase in the h-FABP concentrations produced a current signal that depressed progressively, reaching a saturation up to 50 ng/mL. Figure 5b exhibits the derived calibration curve and a good liner correlation, with R^2 = 0.992, was obtained between the current signal and h-FABP concentrations from 0.5 pg/mL to 50 ng/ mL, and the lowest detection limit was approximately 0.1 pg/mL (S/N = 3). Then, a comparison of the presented liposome-based PEC immunoassay with other obtained detection methods for the determination of h-FABP is listed in Table S1. Our developed PEC immunoassay is superior to most reported bioanalysis. The reproducibility of the PEC biosensor was studied via testing three electrodes with 1 ng/mL of h-FABP. The relative standard deviation was 8.6 %, suggesting an acceptable reproducibility. Figure 5c reveals the photocurrent response stability of the ALP-modulation Au NC@TiO_2 NT electrode, corresponding to 1.0 ng/mL of h-FABP under several repeated on-off irradiations over 380 s. The current signal intensity and shape exhibit

little fluctuation, indicating the steady signal output of this PEC biosensor. Furthermore, the selectivity of the proposed immunoassay to h-FABP was then studied. The common protein species, such as carcinoembryonic antigen (CEA), cardiac troponin T (cTnT), immunoglobulin G (IgG), immunoglobulin A (IgA), P53, and lipoprotein-associated phosPhohPaseA2 (LpPLA2), were investigated as the control. The results as shown in Figure 5d, which illustrates that these proteins trigger a negligible decrease in the signal, suggesting a satisfactory selectivity.

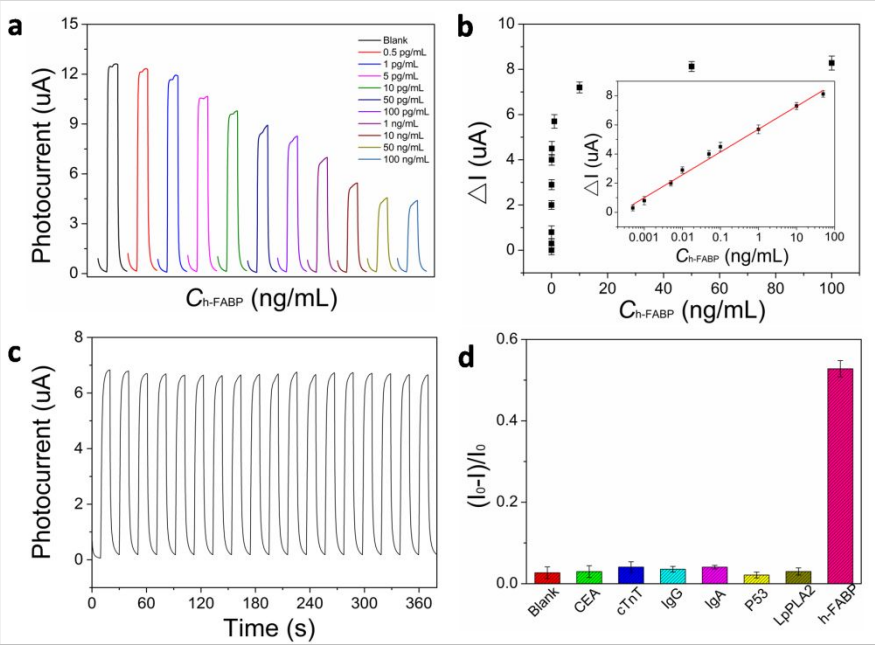

Figure 5. (a) Photocurrent responses of the electrode to different concentrations of h-FABP, (b) corresponding calibration curve. (c) Stability of the Au NC@TiO_2 NTs after incubation with the liposome lysis solution, corresponding to 1.0 ng/mL h-FABP under repeated on-off irradiation within 380 s. (d) Selectivity of the proposed immunoassay to h-FABP (1.0 ng/mL) by comparing it to the interfering proteins at the 10 ng/mL level: CEA, cTnT, IgG, IgA, P53, and LpPLA2. ΔI represents the determined current signal intensity decrement toward the different concentrations of h-FABP. I_0 and I represent the determined current signal intensities of the Au NC@TiO_2 NT electrode before and after ALP catalytic action.

CONCLUSION

In summary, we have described the proof-of-concept study for liposomes-assisted enzymatic modulation of the plasmonic PEC bioanalysis. On the basis of the

ALP-loaded liposomal immunoreaction and Au NCs@TiO_2 NTs photoelectrode, the catalytic growth of the AuNCs and the corresponding signaling mechanism were systematically characterized by SEM, TEM, EDS, DLS, Zeta potentials, XPS, XRD, and UV-vis DRS. In the immunoassay of h-FABP, the signal change could be correlated to target concentration with good analytical performance in terms of sensitivity and selectivity. This study featured the liposomal-assisted modulation of the plasmonic photoelectrode, which is envisioned to inspire more interest in the development of advanced PEC bioanalysis.

ASSOCIATED CONTENT

Supporting Information

Additional information as noted in text. Chemicals, apparatus, synthesis of Au NCs; preparation of TiO_2 NTs, the plot of $(Ahv)^2$ against hv to determine the band gap of the Au NCs, Zeta potential at different pH values of Au NCs, the DLS of bare liposome and ALP-loaded liposome, the caculation of the characteristics of liposome, photocurrent response of Au NC@TiO_2 NT electrode toward various species, and comparison of the published methods for h-FABP determination.

Notes

The authors declare no competing financial interest.

ACKNOWLEDGMENTS

This work was supported by the National Natural Science Foundation of China (nos. 21976129, 21974060, and 21575097) and the Zhejiang Province Public Welfare Technology Application Research Project (no. LGF19B050002).

REFERENCE

(1) Zhao, W.-W.; Xu, J.-J.; Chen, H.-Y. Photoelectrochemical Immunoassays. *Anal. Chem.* **2018**, 90, 615-627.

(2) Shu, J.; Tang, D. Recent Advances in Photoelectrochemical Sensing: From Engineered Photoactive Materials to Sensing Devices and Detection Modes. *Anal. Chem.* **2020**, 92, 363-377.

(3) Tang, J.; Xiong, P.; Cheng, Y.; Chen, Y.; Peng, S.; Zhu, Z.-Q. Enzymatic oxydate-triggered AgNPs etching: A Novel Signal-on Photoelectrochemical Immunosensing Platform Based on Ag@AgCl Nanocubes Loaded RGO Plasmonic Heterostructure. *Biosens. Bioelectron.* **2019**, 130, 125-131.

(4) Yang, R.; Zou, K.; Zhang, X.; Du, C.; Chen, J. A New Photoelectrochemical Immunosensor for Ultrasensitive Assay of Prion Protein Based on Hemin-Induced Photocurrent Direction Switching. *Biosens. Bioelectron.* **2019**, 132, 55-61.

(5) Dai, H.; Zhang, S.; Hong, Z.; Lin, Y. A Potentiometric Addressable Photoelectrochemical Biosensor for Sensitive Detection of Two Biomarkers. *Anal. Chem.* **2016**, 88, 9532-9538.

(6) Zeng, X.; Tu, W.; Li, J.; Bao, J.; Dai, Z. Photoelectrochemical Biosensor Using Enzyme-Catalyzed in Situ Propagation of CdS Quantum Dots on Graphene Oxide. *ACS Appl. Mater. Inter.* **2014**, 6, 16197-16203.

(7) Li, X.; Wang, X.; Zhang, L.; Gong, J. High-Throughput Signal-On Photoelectrochemical Immunoassay of Lysozyme Based on Hole-Trapping Triggered by Disintegrating Bioconjugates of Dopamine-Grafted Silica Nanospheres. *ACS Sensors* **2018**, 3, 1480-1488.

(8) Hu, C.; Zheng, J.; Su, X.; Wang, J.; Wu, W.; Hu, S. Ultrasensitive All-Carbon Photoelectrochemical Bioprobes for Zeptomole Immunosensing of Tumor Markers by an Inexpensive Visible Laser Light. *Anal. Chem.* **2013**, 85, 10612-10619.

(9) Fan, G.-C.; Ma, L.; Jayachandran, S.; Li, Z.; Luo, X. Separating Photoanode From Recognition Events: Toward A General Strategy for a Self-Powered Photoelectrochemical Immunoassay With Both High Sensitivity and Anti-Interference

Capabilities. *Chem. Commun.* **2018**, 54, 7062-7065.

(10) Lin, Y.; Zhou, Q.; Tang, D. Dopamine-Loaded Liposomes for in-Situ Amplified Photoelectrochemical Immunoassay of AFB1 to Enhance Photocurrent of Mn^{2+}-Doped $Zn_3(OH)_2V_2O_7$ Nanobelts. *Anal. Chem.* **2017**, 89, 11803-11810.

(11) Xue, H.; Zhao, J.; Zhou, Q.; Pan, D.; Zhang, Y.; Zhang, Y.; Shen, Y. Boosting the Sensitivity of a Photoelectrochemical Immunoassay by Using SiO_2@polydopamine Core-Shell Nanoparticles as a Highly Efficient Quencher. *ACS Appl. Nano Mater.* **2019**, 2, 1579-1588.

(12) Fan, D.; Bao, C.; Liu, X.; Wu, D.; Zhang, Y.; Wang, H.; Du, B.; Wei, Q. A Novel Label-Free Photoelectrochemical Immunosensor Based on Ncqds and Bi_2S_3 Co-Sensitized Hierarchical Mesoporous Sno_2 Microflowers for Detection of NT-Probnp. *J. Mater. Chem. B* **2018**, 6, 7634-7642.

(13) Da, P.; Li, W.; Lin, X.; Wang, Y.; Tang, J.; Zheng, G. Surface Plasmon Resonance Enhanced Real-Time Photoelectrochemical Protein Sensing by Gold Nanoparticle-Decorated TiO_2 Nanowires. *Anal. Chem.* **2014**, 86, 6633-6639.

(14) Zhang, G.; Shan, D.; Dong, H.; Cosnier, S.; Al-Ghanim, K. A.; Ahmad, Z.; Mahboob, S.; Zhang, X. DNA-Mediated Nanoscale Metal-Organic Frameworks for Ultrasensitive Photoelectrochemical Enzyme-Free Immunoassay. *Anal. Chem.* **2018**, 90, 12284-12291.

(15) Zhou, Q.; Li, G.; Chen, K.; Yang, H.; Yang, M.; Zhang, Y.; Wan, Y.; Shen, Y.; Zhang, Y. Simultaneous Unlocking Optoelectronic and Interfacial Properties of C60 for Ultrasensitive Immunosensing by Coupling to Metal-Organic Framework. *Anal. Chem.* **2020**, 92, 983-990.

(16) Zhu, Y.-C.; Zhang, N.; Ruan, Y.-F.; Zhao, W.-W.; Xu, J.-J.; Chen, H.-Y. Alkaline Phosphatase Tagged Antibodies on Gold Nanoparticles/TiO_2 Nanotubes Electrode: A Plasmonic Strategy for Label-Free and Amplified Photoelectrochemical Immunoassay. *Anal. Chem.* **2016**, 88, 5626-5630.

(17) Gong, L.; Dai, H.; Zhang, S.; Lin, Y. J. A. c. Silver Iodide-Chitosan Nanotag Induced Biocatalytic Precipitation for Self-Enhanced Ultrasensitive Photocathodic Immunosensor. *Anal. Chem.* **2016**, 88, 5775-5782.

(18) Shu, J.; Qiu, Z.; Zhuang, J.; Xu, M.; Tang, D. In Situ Generation of Electron Donor to Assist Signal Amplification on Porphyrin-Sensitized Titanium Dioxide Nanostructures for Ultrasensitive Photoelectrochemical Immunoassay. *ACS Appl. Mater. Inter.* **2015**, 7, 23812-23818.

(19) Al-Jamal, W. T.; Kostarelos, K. Liposomes: From a Clinically Established Drug Delivery System to A Nanoparticle Platform for Theranostic Nanomedicine. *Accounts Chem. Res.* **2011**, 44, 1094-1104.

(20) Qian, R.; Cao, Y.; Long, Y. T. Dual-Targeting Nanovesicles for In Situ Intracellular Imaging of and Discrimination between Wild-type and Mutant p53. *Angew. Chem. Int. Edit.* **2016**, 55, 719-723.

(21) Kong, F.; Zhang, X.; Zhang, H.; Qu, X.; Chen, D.; Servos, M.; Mäkilä, E.; Salonen, J.; Santos, H. A.; Hai, M. Inhibition of Multidrug Resistance of Cancer Cells by Co-Delivery of DNA Nanostructures and Drugs Using Porous Silicon Nanoparticles@ Giant Liposomes. *Adv. Funct. Mater.* **2015**, 25, 3330-3340.

(22) Mazur, F.; Bally, M.; Städler, B.; Chandrawati, R. Liposomes and lipid bilayers in biosensors. *Adv. Colloid interfac.* **2017**, 249, 88-99.

(23) Irby, D.; Du, C.; Li, F. Lipid-Drug Conjugate for Enhancing Drug Delivery. *Mol. Pharmaceut.* **2017**, 14, 1325-1338.

(24) Lee, S.; Koo, H.; Na, J. H.; Lee, K. E.; Jeong, S. Y.; Choi, K.; Kim, S. H.; Kwon, I. C.; Kim, K. DNA Amplification in Neutral Liposomes for Safe and Efficient Gene Delivery. *ACS Nano* **2014**, 8, 4257-4267.

(25) Lee, J.; Kim, J.; Jeong, M.; Lee, H.; Goh, U.; Kim, H.; Kim, B.; Park, J.-H. Liposome-Based Engineering of Cells to Package Hydrophobic Compounds in Membrane Vesicles for Tumor Penetration. *Nano Lett.* **2015**, 15, 2938-2944.

(26) Zhou, J.; Wang, Q.-x.; Zhang, C.-y. Liposome-Quantum Dot Complexes Enable Multiplexed Detection of Attomolar Dnas Without Target Amplification. *J. Am. Chem. Soc.* **2013**, 135, 2056-2059.

(27) Du, Y.; Liang, X.; Li, Y.; Sun, T.; Xue, H.; Jin, Z.; Tian, J. Liposomal Nanohybrid Cerasomes Targeted to PD-L1 Enable Dual-Modality Imaging and Improve Antitumor Treatments. *Cancer Lett.* **2018**, 414, 230-238.

(28) Chen, L.-J.; Yang, C.-X.; Yan, X.-P. Liposome-Coated Persistent Luminescence Nanoparticles as Luminescence Trackable Drug Carrier for Chemotherapy. *Anal. chem.* **2017**, 89, 6936-6939.

(29) Dong, S.; Teo, J. D. W.; Chan, L. Y.; Lee, C.-L. K.; Sou, K. Far-Red Fluorescent Liposomes for Folate Receptor-Targeted Bioimaging. *ACS Appl. Nano Mater.* **2018**, 1, 1009-1013.

(30) Mei, L.-P.; Liu, F.; Pan, J.-B.; Zhao, W.-W.; Xu, J.-J.; Chen, H.-Y. Enediol-Ligands-Encapsulated Liposomes Enables Sensitive Immunoassay: A Proof-Of-Concept for General Liposomes-Based Photoelectrochemical Bioanalysis. *Anal. Chem.* **2017**, 89, 6300-6304.

(31) Zhuang, J.; Han, B.; Liu, W.; Zhou, J.; Liu, K.; Yang, D.; Tang, D. Liposome-Amplified Photoelectrochemical Immunoassay for Highly Sensitive Monitoring of Disease Biomarkers Based on A Split-Type Strategy. *Biosens. Bioelectron.* **2018**, 99, 230-236.

(32) Wei, J.; Chen, H.; Chen, H.; Cui, Y.; Qileng, A.; Qin, W.; Liu, W.; Liu, Y. Multifunctional Peroxidase-Encapsulated Nanoliposomes: Bioetching-Induced Photoelectrometric and Colorimetric Immunoassay for Broad-Spectrum Detection of Ochratoxins. *ACS Appl. Mater. Inter.* **2019**, 11, 23832-23839.

(33) Kang, Z.; Yan, X.; Wang, Y.; Zhao, Y.; Bai, Z.; Liu, Y.; Zhao, K.; Cao, S.; Zhang, Y. Self-Powered Photoelectrochemical Biosensing Platform Based on Au NPs@ ZnO Nanorods Array. *Nano Res.* **2016**, 9, 344-352.

(34) Zhang, Y.; Shoaib, A.; Li, J.; Ji, M.; Liu, J.; Xu, M.; Tong, B.; Zhang, J.; Wei, Q. Plasmon Enhanced Photoelectrochemical Sensing Of Mercury (II) Ions in Human Serum Based on Au@Ag Nanorods Modified TiO_2 Nanosheets Film. *Biosens. Bioelectron.* **2016**, 79, 866-873.

(35) Li, R.; Yan, R.; Bao, J.; Tu, W.; Dai, Z. A Localized Surface Plasmon Resonance-Enhanced Photoelectrochemical Biosensing Strategy For Highly Sensitive and Scatheless Cell Assay Under Red Light Excitation. *Chem. Commun.* **2016**, 52, 11799-11802.

(36) Wang, Y.; Su, H.; Xu, C.; Li, G.; Gell, L.; Lin, S.; Tang, Z.; Häkkinen, H.;

Zheng, N. An Intermetallic $Au_{24}Ag_{20}$ Superatom Nanocluster Stabilized By Labile Ligands. *J. Am. Chem. Soc.* **2015**, 137, 4324-4327.

(37) Li, G.; Jin, R. Atomically Precise Gold Nanoclusters as New Model Catalysts. *AccountsChem. Res.* **2013**, 46, 1749-1758.

(38) Xiao, F.-X.; Zeng, Z.; Liu, B. Bridging the Gap: Electron Relay and Plasmonic Sensitization of Metal Nanocrystals for Metal Clusters. *J. Am. Chem. Soc.* **2015**, 137, 10735-10744.

(39) Zhang, J.; Tu, L.; Zhao, S.; Liu, G.; Wang, Y.; Wang, Y.; Yue, Z. Fluorescent Gold Nanoclusters Based Photoelectrochemical Sensors for Detection of H_2O_2 and Glucose. *Biosens. Bioelectron.* **2015**, 67, 296-302.

(40) Smolina, K.; Wright, F. L.; Rayner, M.; Goldacre, M. J. Long-Term Survival and Recurrence After Acute Myocardial Infarction in England, 2004 to 2010. *Circ-Cardiovasc Qual*, **2012**, 5, 532-540.

(41) Stan, D.; Mihailescu, C.-M.; Iosub, R.; Moldovan, C.; Savin, M.; Baciu, I. Electrochemical Studies of Homogeneous Self-Assembled Monolayers Versus Mixed Self-Assembled Monolayers on Gold Electrode for "Label Free" Detection of Heart Fatty Acid Binding Protein. *Thin Solid Films* **2012**, 526, 143-149.

(42) Guo, X.; Zong, L.; Jiao, Y.; Han, Y.; Zhang, X.; Xu, J.; Li, L.; Zhang, C.-w.; Liu, Z.; Ju, Q.; Liu, J.; Xu, Z.; Yu, H.-D.; Huang, W. Signal-Enhanced Detection of Multiplexed Cardiac Biomarkers by a Paper-Based Fluorogenic Immunodevice Integrated with Zinc Oxide Nanowires. *Anal. Chem.* **2019**, 91, 9300-9307.

(43) Peurifoy, S. R.; Russell, J. C.; Sisto, T. J.; Yang, Y.; Roy, X.; Nuckolls, C. Designing Three-Dimensional Architectures for High-Performance Electron Accepting Pseudocapacitors. *J. Am. Chem. Soc.* **2018**, 140, 10960-10964.

(44) Chen, F.-Z.; Zhu, Y.-C.; Han, D.-M.; Chen, H.-Y. Three-Dimensional ZnInS Nanoflakes@Carbon Fiber Frameworks for Biocatalytic Precipitation-Based Photoelectrochemical Immunoassay. *ACS Appl. Bio Mater.* **2020**, 3, 1761-1768.

(45) Zhang, Z.; Zhang, L.; Hedhili, M. N.; Zhang, H.; Wang, P. Plasmonic Gold Nanocrystals Coupled with Photonic Crystal Seamlessly on TiO_2 Nanotube Photoelectrodes for Efficient Visible Light Photoelectrochemical Water Splitting.

Nano Lett. **2013**, 13, 14-20.

(46) Xie, Q.; Wang, Z.; Huang, Y.; Bi, X.; Zhou, H.; Lin, M.; Yu, Z.; Wang, Y.; Ni, N.; Sun, J. Characterization of Human Ethmoid Sinus Mucosa Derived Mesenchymal Stem Cells (hESMSCs) and the Application of hESMSCs Cell Sheets in Bone Regeneration. *Biomaterials* **2015**, 66, 67-82.

(47) Zhang, Q.; Dong, H.; Li, Y.; Zhu, Y.; Zeng, L.; Gao, H.; Yuan, B.; Chen, X.; Mao, C. Microgrooved Polymer Substrates Promote Collective Cell Migration to Accelerate Fracture Healing in an in Vitro Model. *ACS Appl. Mater. Inter.* **2015**, 7, 23336-23345.

(48) Xiao, F. X.; Hung, S. F.; Miao, J.; Wang, H. Y.; Yang, H.; Liu, B. Metal-Cluster-Decorated TiO_2 Nanotube Arrays: A Composite Heterostructure toward Versatile Photocatalytic and Photoelectrochemical Applications. *Small* **2015**, 11, 554-567.

(49) Li, H.; Bian, Z.; Zhu, J.; Huo, Y.; Li, H.; Lu, Y. Mesoporous Au/TiO_2 Nanocomposites with Enhanced Photocatalytic Activity. *J. Am. Chem. Soc.* **2007**, 129, 4538-4539.

TOC